Journal of Chromatography B 1269 (2026) 124861

Contents lists available at ScienceDirect

Journal of Chromatography B

journal homepage: www.elsevier.com/locate/jchromb

# Identification of potential TMPRSS2 inhibitors via high-throughput screening based on oriented immobilized cell membrane chromatography technology

Siqi Wang [a,1], Min Si [b,1], Qihuan Liao [a], Yifei Li [a], Wenyu Yang [a], Huaizhen He [a], Cheng Wang [a,*]

[a] School of Pharmacy, Xi'an Jiaotong University, Xi'an, Shaanxi 710061, China
[b] Xi'an Hospital of Traditional Chinese Medicine, Xi'an, Shaanxi 710021, China

ARTICLE INFO

*Keywords:*
TMPRSS2
Cell membrane chromatography
SMA copolymer
His-tag
Inhibitor screening

ABSTRACT

The transmembrane protease serine 2 (TMPRSS2) plays a crucial role in the cellular entry of coronaviruses, making the search for its inhibitors pertinent for developing novel antiviral drugs. Cell membrane chromatography (CMC) is a novel methodology that immobilizes membrane receptors on silica gel, utilizing chromatographic techniques to discover new drugs. To enhance the accuracy of this method, this study employed styrene-maleic acid (SMA) copolymers for protein extraction His-tag for protein immobilization, which would minimize alterations to the biological structure of TMPRSS2. Methodological validation demonstrated that this model offers improved reproducibility and longer column lifespan compared to traditional CMC columns, alongside superior screening performance. Utilizing this model, a screening campaign was conducted against a commercial small molecule library containing 3010 compounds. Preliminary activity validation revealed that the screened famotidine and TS0665 effectively inhibited pseudovirus infection of cells. These findings provide an experimental foundation for the subsequent development of antiviral therapeutics.

## 1. Introduction

Coronaviruses primarily invade host cells via the membrane fusion pathway, leading to pneumonia characterized by high infection rate and severe symptoms, which poses a significant threat to global human health [1]. Studies indicate that TMPRSS2 plays a critical role in the membrane fusion process [2]. It cleaves two key spike proteins of the coronavirus, thereby activating the virus and facilitating its fusion with target cells [3,4]. Consequently, developing TMPRSS2 inhibitors represents a promising strategy for identifying therapeutic agents against coronaviruses [5].

Currently known TMPRSS2 inhibitors include camostat [6] and nafamostat [7]. Camostat, a serine protease inhibitor, exhibits potent antiviral activity by targeting TMPRSS2 [8,9]. Nafamostat, another small-molecule serine protease inhibitor, is clinically used as an anticoagulant [10] and has demonstrated efficacy against both type A influenza and coronaviruses. However, no TMPRSS2 inhibitor has yet shown significant clinical benefits in alleviating COVID-19 symptoms [11]. Hence, discovering novel TMPRSS2 inhibitors remains of great practical importance.

Common methods for screening membrane protein targets include virtual screening [12], fluorescence-based assays [13], and in vitro immobilized membrane protein screening [14]. Virtual screening may not always reflect actual binding interactions, while fluorescence-based methods are often limited in scalability and are unsuitable for high-throughput applications [15].

The concept of screening using membrane proteins in vitro originated from the field of 'bionics', introduced by Otto Schmitt [16], with the aim of constructing functional models that mimic biological systems to address complex biomedical challenges. Notably, approximately 45 % of medicines exert their therapeutic effects by binding to receptor proteins located on the cell membrane [17]. By simulating this binding

*Abbreviations:* Caco2, Human intestinal epithelial cells; Calu-3, Cultured human airway epithelial cells; DMSO, Dimethyl sulfoxide; HEK293T, Human embryonic kidney 293 T; SARS-CoV-2, Severe acute respiratory syndrome coronavirus 2; SEM, Scanning electron microscope; TMPRSS2, Transmembrane serine protease 2; VS, Vinyl sulfone; PBS, Phosphate buffered saline..

* Corresponding author.
*E-mail address:* chengwang@xjtu.edu.cn (C. Wang).
[1] These authors contributed equally to this work.

https://doi.org/10.1016/j.jchromb.2025.124861
Received 28 September 2025; Received in revised form 5 November 2025; Accepted 17 November 2025
Available online 19 November 2025
1570-0232/© 2025 Elsevier B.V. All rights are reserved, including those for text and data mining, AI training, and similar technologies.

process in vitro, screening accuracy and biological relevance can be significantly enhanced.

Cell membrane chromatography (CMC) is a biomimetic chromatographic method that can determine the binding characteristics between ligands and membrane receptors [18,19], and identify specific target components in a complex sample [20,21]. With the rapid development of receptor overexpression technology, engineered cell cultures, and immobilization strategy of membrane receptors, CMC technology has made significant progress over the past 30 years. However, due to the presence of large-molecular-weight protein tags and non-target proteins, the stability, selectivity and specificity of CMC are still compromised [22]. To address these issues, the extraction and functional immobilization of membrane proteins constitute two critically important steps in optimizing the screening platform.

Traditional detergent-based extraction may disrupt membrane protein structures and introduce experimental bias [23,24], Furthermore, different membrane proteins often require specific detergents for extraction—a process that typically involves extensive empirical screening. In contrast, amphiphilic copolymers such as styrene-maleic acid (SMA) [25,26] offer a more efficient and generalizable alternative. At pH 7–8, the hydrophobic segments bind to membrane proteins, excising them along with their native lipid environment, while the hydrophilic segments face outward, forming water-soluble SMA lipid particles (SMALPs). This approach preserves the native protein structure and improves screening reliability.

Although SMALPs can be adsorbed onto silica gel for protein immobilization [27], this physical adsorption is often unstable, nonspecific, and may lead to inaccurate screening results. To address this, covalent immobilization via chemical modification of silica and protein tagging can be used. However, the commonly used SNAP-tag [28,29], an affinity protein tag, has a relatively large molecular weight, which may interfere with the expression and tertiary structure of the target protein, thereby influencing screening outcomes. It is therefore necessary to select an alternative affinity tag with a lower molecular weight, For example His-tag [30].

In summary, we will optimize the screening model by integrating smaller tag based, His-tag, purification with SMA copolymer extraction technology. This combined approach enables targeted isolation of the receptor while preserving its native conformation, along with stable immobilization onto a solid-phase carrier. These improvements are expected to significantly enhance the specificity and selectivity of the model. The optimized platform will subsequently be applied to screen a small-molecule library, with its reliability further validated through functional activity assays.

## 2. Materials and methods

### 2.1. Chemicals and reagents

Camostat, Levofloxacin, Metformin, Acyclovir, Clonidine was purchased from Yuan Ye Biotechnology Co., Ltd. (Shanghai, China). Acetaminophen, Carbamazepine, Cilitizine, Moroxydine, Famotidine, Cimetidine was purchased from China National Institute for Food and Drug Control (Beijing, China). The small molecule library was purchased from Selleck Bioscience Co., Ltd. (Texas, USA). Methanol (chromatographic pure) was purchased from Thermo Fisher Scientific Co., Ltd. (Shanghai, China).

GAPDH antibody was purchased from SanYing Biotechnology Co., Ltd. (Wuhan, China). TMPRSS2 antibody was purchased from Wuhan ABclonal Technology Co., Ltd. (Wuhan, China). His-tag antibody was purchased from ProteinTech Biosciences Co., Ltd. (Wuhan, China). NaOH was purchased from Xinjinhua Chemical Co., Ltd. (Tianjin, China). Phosphate buffered saline (PBS) was purchased from Wuhan Saiwell Biotechnology Co., Ltd. (Wuhan, China). DMSO was purchased from GuangHua Science & Technology Co., Ltd. (Guangzhou, China). CCK-8 kit was purchased from MiShu Biotechnology Co., Ltd. (Xi'an, China). Fetal bovine serum (FBS) was purchased from Shanghai Newzerum Biotechnology Co., Ltd. (Shanghai, China).DiI membrane dye was purchased from Biyuntian Biotechnology Co., Ltd. (Shanghai, China). Boc-Gln-Ala-Arg-AMC (95 %) was purchased from MedChemexpress Biotechnology Co., Ltd. (Shanghai, China). Poly-L-lysine was purchased from Biyuntian Biotechnology Co., Ltd. (Shanghai, China).

### 2.2. Cell lines

TMPRSS2-His-tag HEK293T cell was constructed by Cyagen Bioscience Inc. (Suzhou, China). Calu-3 cell was purchased from Wuhan Procell Life Science & Technology Co., Ltd. (Wuhan, China). Caco2 cell was gifted from Lu Wen, a teacher of Xi'an Jiaotong University. All cells were cultured in carbon dioxide incubator (Celmate, Esco, Singapore), the condition is 5 % $CO_2$, 37 °C.

### 2.3. Construction and characterization of high-expression TMPRSS2-his-tag HEK293T cells

The generation of HEK293T cells with high expression of TMPRSS2-His-tag was carried out by Cyagen Bioscience Inc. (Suzhou, China). Both negative control HEK293T cells (NC-HEK293T) and TMPRSS2-His-tag-expressing HEK293T cells were cultured and subsequently disrupted to obtain protein samples. The expression of TMPRSS2 was confirmed by using Quantitative Polymerase Chain Reaction (qPCR) and Western Blotting.

### 2.4. Preparation and characterization of SMA and VS silica gel

The SMAnh copolymer were hydrolyzed to yield SMA copolymer, and their chemical structure was confirmed by Fourier transform infrared spectroscopy (FT-IR) (Nicolet iS 50, Yingmei Electronic Technology Co., Ltd., China). Under catalytic conditions, amino silica was reacted with divinyl sulfone for 12 h to obtain VS-functionalized silica (VS silica). The morphological features of the resulting VS silica were characterized using scanning electron microscopy (SEM) (GEMINI 500, Carl Zeiss, Germany).

### 2.5. Preparation and characterization of TMPRSS2-his-tag@VS/CMC stationary phase

TMPRSS2-His-tag HEK293T cells were cultured and disrupted. The resulting membrane fraction was collected by centrifuge and incubated with SMA copolymers for 2 h to form TMPRSS2-containing SMALPs. These SMALPs were then conjugated with VS silica via 12 h incubation, resulting in the preparation of TMPRSS2-His-tag@VS silica stationary phase. The morphology was characterized by using scanning electron microscope (SEM). Adding 200 μL DiI membrane dye into the solution, after 20 mins, photographed under immunofluorescence microscope (Ti-*E*-C2, Nicon, Japan) to verify the biological activity of the fixed phase.

### 2.6. System suitability for TMPRSS2-his-tag@VS silica/CMC model

The TMPRSS2-His-tag@VS silica gel stationary phase was packed into a chromatographic column (2.0 × 10 mm I.D. × L) by packing machine (RPL-10ZD, Ripley Technology Instrument Co., Ltd., China) to prepare the TMPRSS2-His-tag@VS/CMC analytical column. The column was then installed to high-performance liquid chromatography system (LC-2040C 3D, Shimadzu, Japan), sample analysis was carried out at 37 °C with a flow phase of 5 mmol/L $Na_2HPO_4{\cdot}12H_2O$ (pH 7.4) solution, and the flow rate of 0.20 mL/min. The sample injection volume was 5 μL for each sample, and diode array detector was used for full wavelength scanning of the sample.

To ensure the reliability of subsequent screening results, the applicability of the column was thoroughly validated. Both TMPRSS2-

**Table 1**
TMPRSS2 mRNA expression efficiency assay.

| | Human TMPRSS2 | Human GADPH | ΔCT | ΔΔCT | $2^{-\Delta\Delta CT}$ | Expressive efficiency |
|---|---|---|---|---|---|---|
| TMPRSS2-His-tag HEK293T | 20.28 | 17.13 | 3.15 | −13.35 | 10,495.80 | 1,049,580 % |
| NC-HEK293T | 33.41 | 16.91 | 16.50 | 0 | 1 | 100.00% |

positive and TMPRSS2-negative compounds were selected to evaluate the specificity and selectivity of the column. The intro-column repeatability was assessed by performing consecutive injections of the same sample on a single column. Meanwhile, three independently prepared CMC columns were used for parallel sample injections to determine the inter-column repeatability. Furthermore, to evaluate the column lifetime, a freshly prepared CMC column was stored under appropriate conditions and one sample was injected daily over an extended period to monitor the degradation of chromatographic performance.

### *2.7. TMPRSS2-his-tag@VS silica/CMC model screening for potential inhibitory active compounds*

The 3010 compounds in the library were pooled into groups of ten and formulated as 1 mmol/L screening samples. The integrity of the model was monitored by spiking with camostat (positive control) every eight samples. Samples were sorted by their relative retention time to the nearest camostat retention time. From these, mixed samples with the greatest relative retention times were identified, and each of their ten constituent compounds was prepared as a 1 mmol/L single-compound sample for further investigation of their retention profiles on the TMPRSS2-His-tag-CMC model.

### *2.8. TMPRSS2 intracellular enzyme activity assay*

The intracellular proteolytic activity of TMPRSS2 was evaluated using a fluorogenic substrate to identify potential active compounds. The substrate Boc-Gln-Ala-Arg-AMC, which contains a fluorescent AMC group, was employed. Upon cleavage by TMPRSS2 in TMPRSS2-His-tag HEK293T cells, AMC is released,

Added poly-L-lysine to 96-well plate and overnight in incubator. The following day, the poly-L-lysine solution was removed, and the plate was washed twice with PBS. TMPRSS2-His-tag HEK293T cells were seeded at a density of $10^4$ cells per well. After adhesion, the experimental group was added serum-free culture medium with concentration of 25 μmol/L, and the control group was added with an equal of DMSO, then the fluorogenic substrate was added at final concentration of 50 μmol/L, followed by another 24 h of incubation. Subsequently, 65 μL of the supernatant from each well was transferred to a black 96-well plate, and fluorescence intensity was measured at room temperature using multifunctional microplate detection (BioTek Synergy Neo2, Agilent, USA), with excitation at 380 nm and emission at 460 nm.

### *2.9. Computer aided molecular docking*

The interaction between small molecules and TMPRSS2 protein was simulated using the computational software SYBYL-X 2.0. The procedure was as follows: retired the three-dimensional structure of TMPRSS2 from the Protein Data Bank (PDB ID: 7MEQ) and imported into SYBYL. Then sketch the structures of the small molecules within the software and subsequently energy-minimized. Molecular docking simulations were performed using the corresponding software module. The resulting poses were analyzed to determine whether each ligand was positioned within the protein's active site, whether hydrogen bonds were formed with key amino acid residues, and to evaluate the number and distances of these hydrogen bonds.

### *2.10. Cell viability assay*

Cells were seeded in 96-well plates at an appropriate density (Calu-3 cells: $10^5$ per well, Caco2 cells: $8 \times 10^5$ per well), no cells in blank group. After adhesion, the experimental groups were treated with TS0665 and famotidine at indicated final concentrations (Calu-3 cells: 1, 2, 5, 10, 20, 50, 100 μmol/L; Caco2 cells: 1, 2, 5, 10, 20, 50, 100 μmol/L, 1, 5, 10, 20, 50, 100, 200 μmol/L), while the control and blank groups received 10 μL of serum-free medium. Following 24 h of incubation, 10 μL of CCK-8 solution was added to each well, mixed gently, and incubated for 1 h. The absorbance at 450 nm ($OD_{450\ nm}$) was measured using microplate reader (BioTek, USA) and cell viability was calculated using the following formula:

$$\text{Cell viability rate} = (OD_{\text{Ttrated}} - OD_{\text{Blank}})/(OD_{\text{Control}} - OD_{\text{Blank}}) \times 100\%$$

### *2.11. Investigation of the time of infection with pseudo virus*

Calu-3 and Caco-2 cells were seeded in 96-well plates at logarithmic growth phase. After adhesion, 1 μL of SARS-CoV-2 pseudovirus was added to each well. The culture medium was replaced at 8, 24, and 48 hpost-infection, followed by an additional 48-h incubation period. Subsequently, 30 μL of cell lysis solution was added to each well, and the plate was gently agitated. Following lysis at room temperature for approximately 3 min, 50 μL of luciferase substrate solution was added, and luciferase activity was measured using multifunctional microplate detection instrument in luminescence mode at a wavelength of 560 nm with an integration time of 1 s.

### *2.12. Inhibition activity of potential active compounds on infection of Calu-3 and Caco2 cells by SARS-CoV-2 pseudo-virus determined*

Cells were seeded in 96-well plates at an appropriate density (Calu-3 cells: $10^5$ per well, Caco2 cells: $8 \times 10^5$ per well). After adhesion, the experimental groups were treated with TS0665 (10, 20, 50 μmol/L) and famotidine (5, 10, 20, 50 μmol/L), while control groups received an equivalent volume of compound-free culture medium. Following 2 h of incubation, 1 μL of SARS-CoV-2 pseudovirus was added to each well. Then Calu-3 cells were incubated for 8 h, and Caco-2 cells were incubated for 24 h. Subsequently, the supernatant was removed and replaced with fresh MEM medium supplemented with 10 % FBS. After 48 h of additional culture, luciferase activity in each well was measured using multifunctional microplate detection instrument in luminescence mode at a wavelength of 560 nm.

### *2.13. Statistical analysis*

Graphpad prism 7 was used for data statistical analysis, and the results were expressed as the mean ± standard deviation. Using *t*-test, $p < 0.05$ represented that the difference was statistically significant. ($^{*}p < 0.05$, $^{**}p < 0.01$, $^{***}p < 0.001$).

## 3. Results and discussion

### *3.1. Preparation and characterization of TMPRSS2-his-tag@VS /CMC stationary phase*

The expression of TMPRSS2 was assessed using qPCR and western

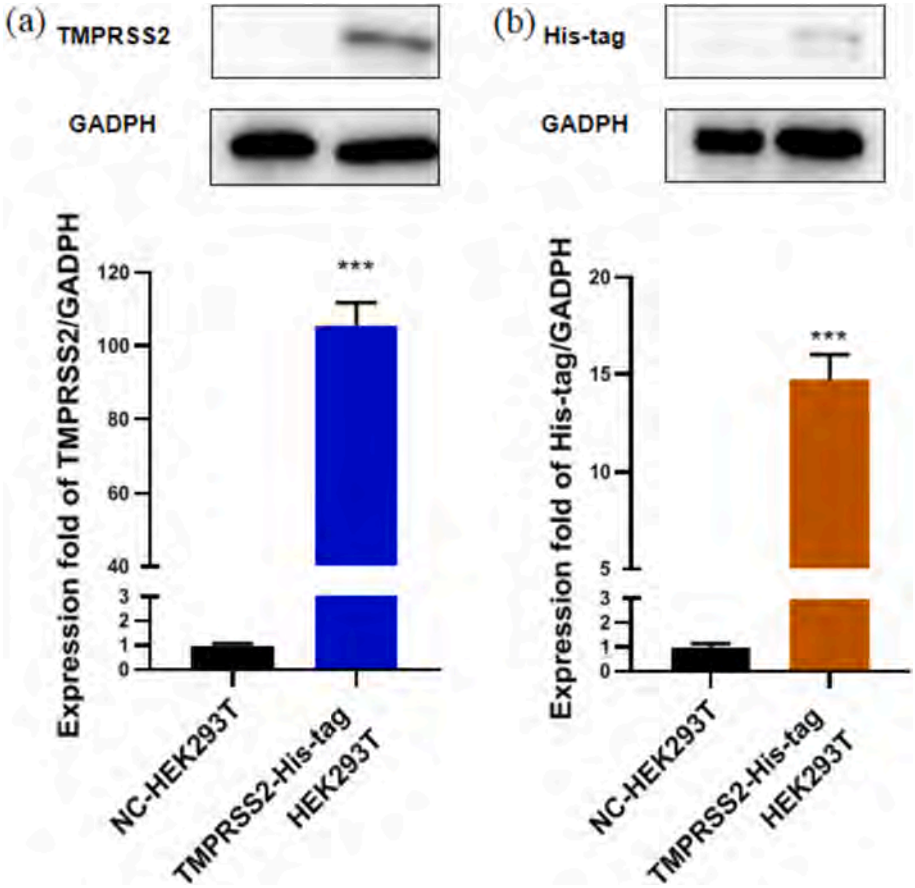


**Fig. 1.** Verification of protein expression in cells. (a): TMPRSS2; (b): His-tag. $^{***}P < 0.001$, n = 3;

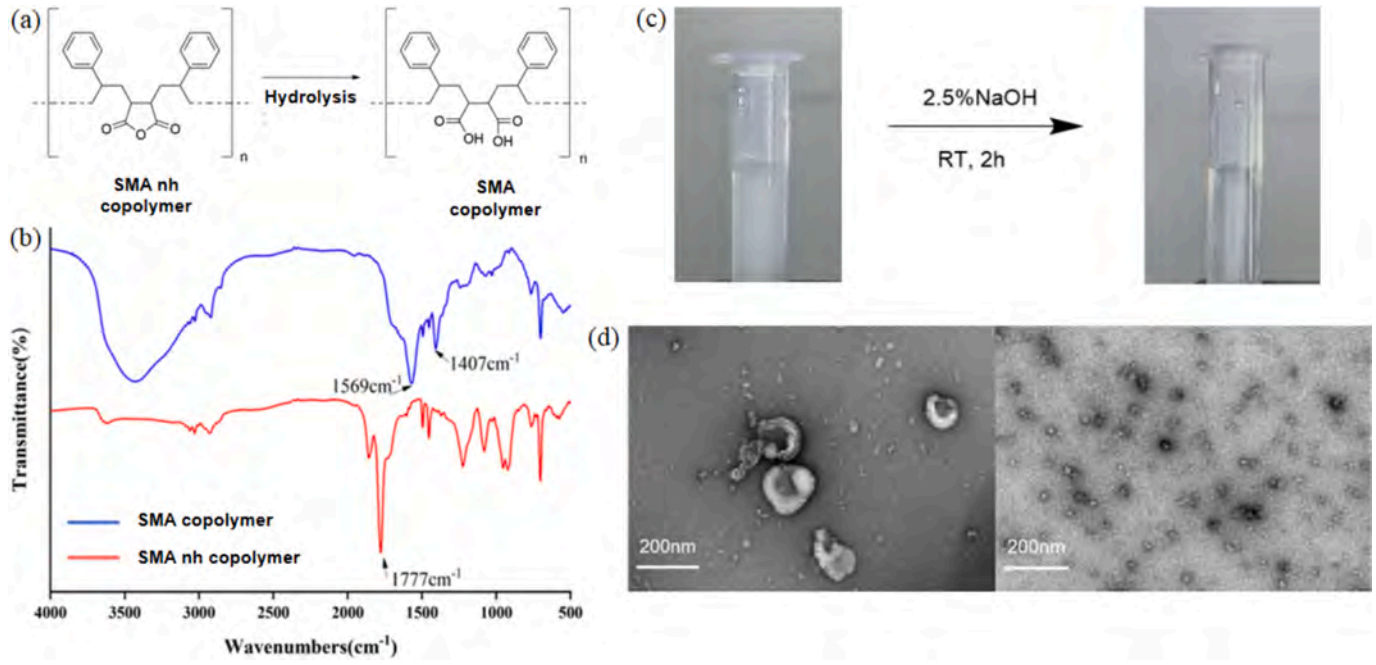


**Fig. 2.** Synthesis of SMA copolymers and extraction of membrane proteins. (a) Hydrolysis of SMAnh copolymers yields SMA copolymers. (b)The FT-IR spectrum of SMAnh copolymers(blue) and SMA copolymers(red). (c) Adding SMA copolymer to extract membrane protein, the membrane solution changed from turbid to clear. (d) The TEM images of the membrane solution before and after the extraction of membrane proteins from SMA copolymers. (For interpretation of the references to colour in this figure legend, the reader is referred to the web version of this article.)

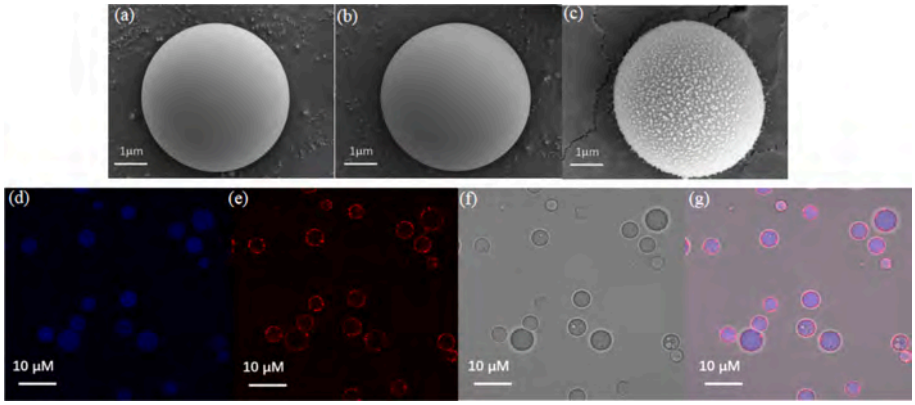


**Fig. 3.** Characterization of the TMPRSS2-His-tag@VS/CMC stationary phase. The SEM images of aminated silica(a), VS silica(b) and the TMPRSS2-His-tag@VS/CMC stationary phase(c). Laser confocal images of TMPRSS2 membrane protein and phospholipid in TMPRSS2-His-tag@VS/CMC stationary phase. (d): DiI membrane dye incubation. (e): Incubation of anti-TMPRSS2 antibodies. (f): lit field. (g) merge.

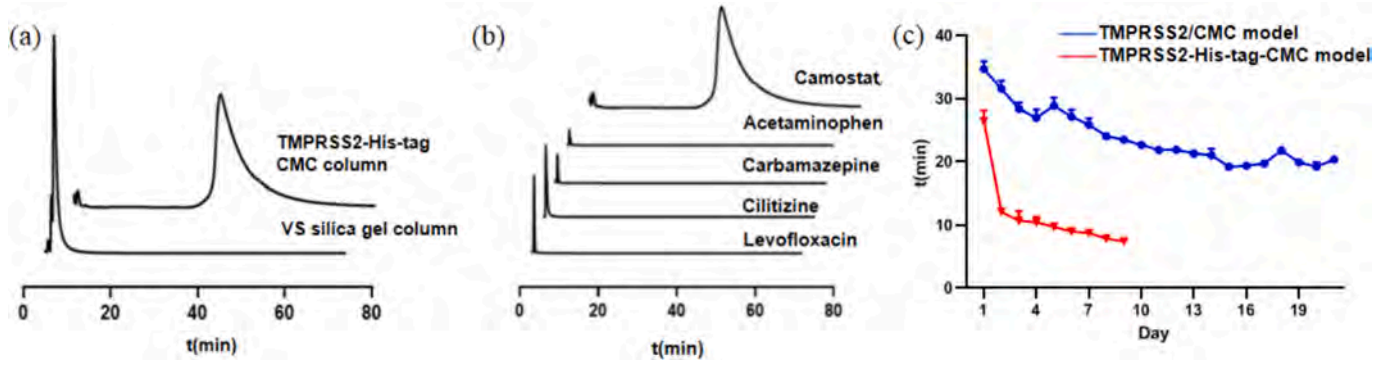


**Fig. 4.** Results of the system adaptability investigation. (a): Specificity. (b): selectivity assessment. (c): repeatability assessment.

Blotting. Compared to NC-HEK293T cells, TMPRSS2-His-tag HEK293T cells exhibited 10,495-fold increase in mRNA expression (Table. 1) and 100-fold increase in protein expression (Fig. 1a). Additionally, His-tag expression was observed to be 15-fold higher (Fig. 1b). These results confirm the successful construction of the TMPRSS2-His-tag HEK293T cell.

The SMAnh copolymer contains maleic anhydride carbonyl groups, which exhibit a characteristic absorption band at 1777 $cm^{-1}$ in FT-IR spectroscopy. Following hydrolysis, these groups are converted into carboxylate carbonyl moieties, as evidenced by the appearance of new absorption peaks at 1569 $cm^{-1}$ and 1407 $cm^{-1}$, confirming the successful synthesis of SMA copolymer (Fig. 2a,b).

Subsequently, cell lysates were treated with the synthesized SMA copolymer to extract membrane proteins. Characterization studies indicated that The SMA copolymer fragments the sheet-like membrane structures, which initially range from 100 to 200 nm in diameter, into uniform nanodisks measuring approximately 10–15 nm. This process significantly improves the solubility of the membrane components in aqueous solution. (Fig. 2c,d).

Aminated silica gel was reacted with divinyl sulfone to yield VS silica gel. The membrane protein extracted by SMA copolymer was conjugated onto VS silica gel to fabricate the TMPRSS2-His-tag@VS/CMC stationary phase. Scanning electron microscopy (SEM) imaging showed that both the aminated silica and VS silica exhibited relatively smooth surface morphologies (Fig. 3a,b), suggesting that divinyl sulfone modification did not significantly alter the surface structure.

Following the coupling of the membrane protein, the initially smooth surface of the VS silica gel became coated with a thin, film-like layer, accompanied by a homogeneous distribution of fine particulate structures, indicating successful immobilization of the protein-loaded nanodisks (Fig. 3c). Furthermore, immunofluorescence and confocal microscopy analyses confirmed that the TMPRSS2 protein immobilized on the stationary phase retained its biological activity and was uniformly distributed (Fig. 3d-g).

These results demonstrate that incorporating a His-tag into TMPRSS2, functionalizing aminated silica with divinyl sulfone, and employing SMA copolymer for membrane protein extraction enable precise and efficient protein immobilization onto silica surfaces while preserving bioactivity. This approach establishes a robust foundation for subsequent experimental applications.

**Table 2**
Repeatability investigation of TMPRSS2-His-tag-CMC model and TMPRSS2/CMC model.

| Repeatability within the column | | | Between-column repeatability | | |
|---|---|---|---|---|---|
| Number | $R_1$ | $R_2$ | Number | $R_3$ | $R_4$ |
| 1 | 34.73 | 27.37 | 1 | 34.44 | 27.43 |
| 2 | 34.36 | 25.62 | 2 | 35.02 | 24.33 |
| 3 | 34.44 | 25.38 | 3 | 34.62 | 24.83 |
| 4 | 34.21 | 24.99 | | | |
| 5 | 33.60 | 23.46 | | | |
| RSD (%) | 1.22 | 5.53 | | 0.86 | 6.52 |

R1 and R3 are the retention times of camostat mesylate on the TMPRSS2-His-tag-CMC model, R2,R4 are the retention times of camostat mesylate on the traditional physical adsorption TMPRSS2/CMC model.

### 3.2. Evaluation and application of a TMPRSS2-his-tag-CMC model

The TMPRSS2-His-tag@VS/CMC column was prepared by wet

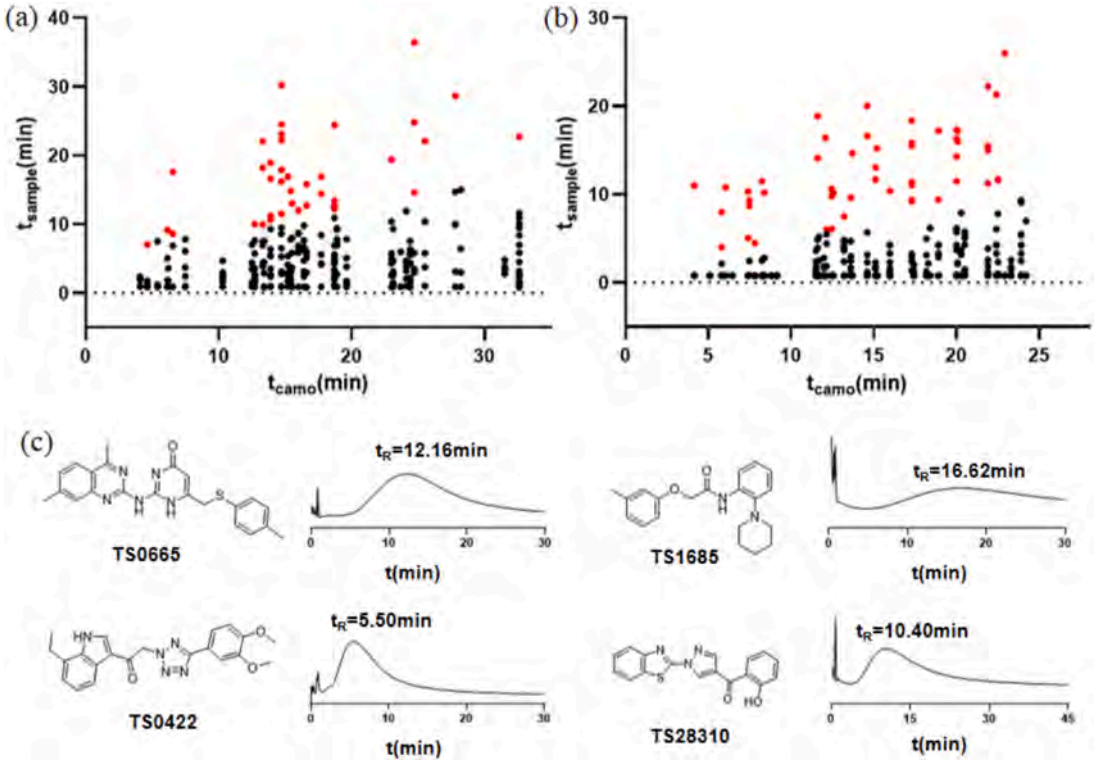


**Fig. 5.** The screening results of the TMPRSS2-His-tag CMC model for small molecule compound libraries. (a): Horizontal axis $t_{camo}$ represents retention time of positive nedicine with the shortest analysis time, and vertical axis $t_{sample}$ represents retention time of sample. Mixed screened samples with $t_{sample}/t_{camo}$ greater than 1/2 are used for second round of screening and are represented by red dots. (b): Single screening results.Samples with $t_{sample}/t_{camo}$ greater than 1/2 were used for activity screening and indicated by red dots. (c): Chemical structures and chromatograms of some compounds. (For interpretation of the references to colour in this figure legend, the reader is referred to the web version of this article.)

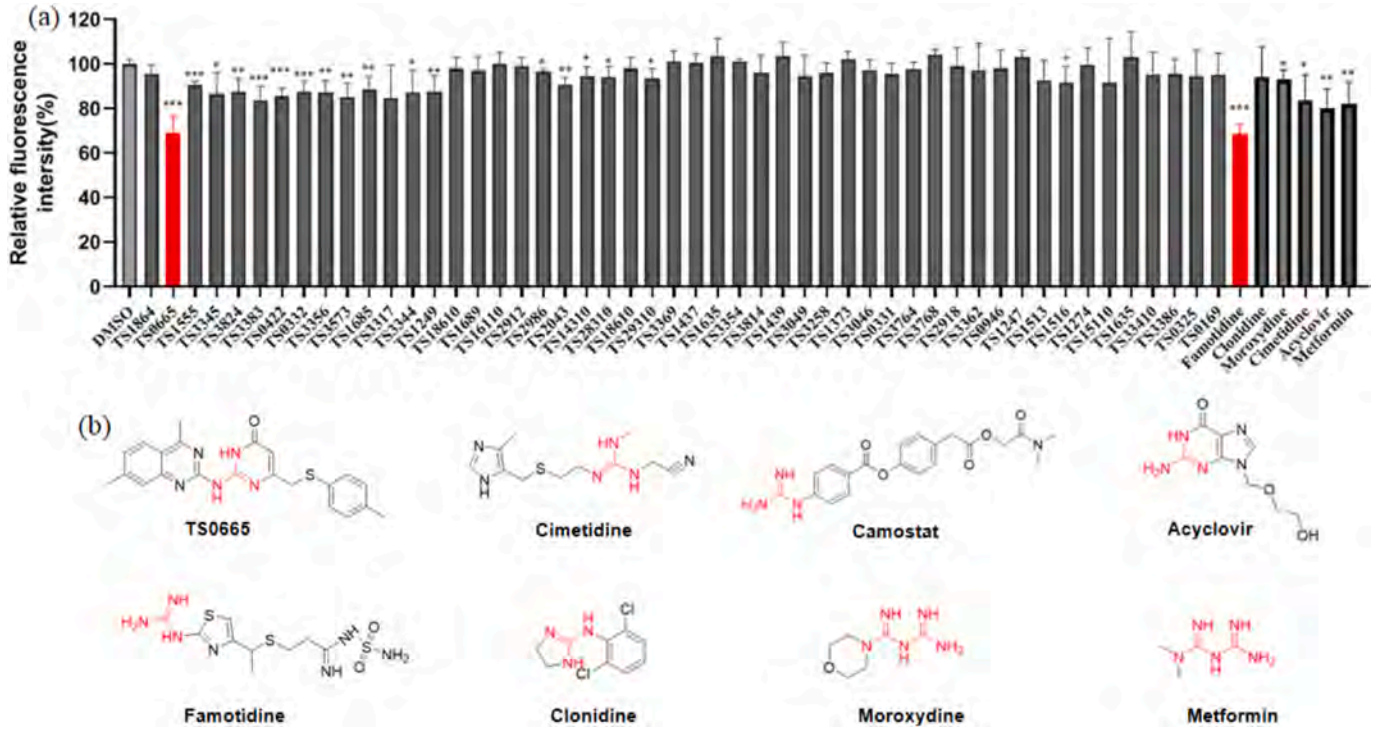


**Fig. 6.** The results of intracellular enzyme activity inhibition of compounds and some structural diagrams. (a): Intracellular enzyme activity inhibition results of the retained compound TMPRSS2 in the TMPRSS2-His-tag CMC model. (B): Structure of guanidine-containing medicines. Compared with the control group. $^{*}P < 0.05$, $^{***}P < 0.001$, $n = 5$.

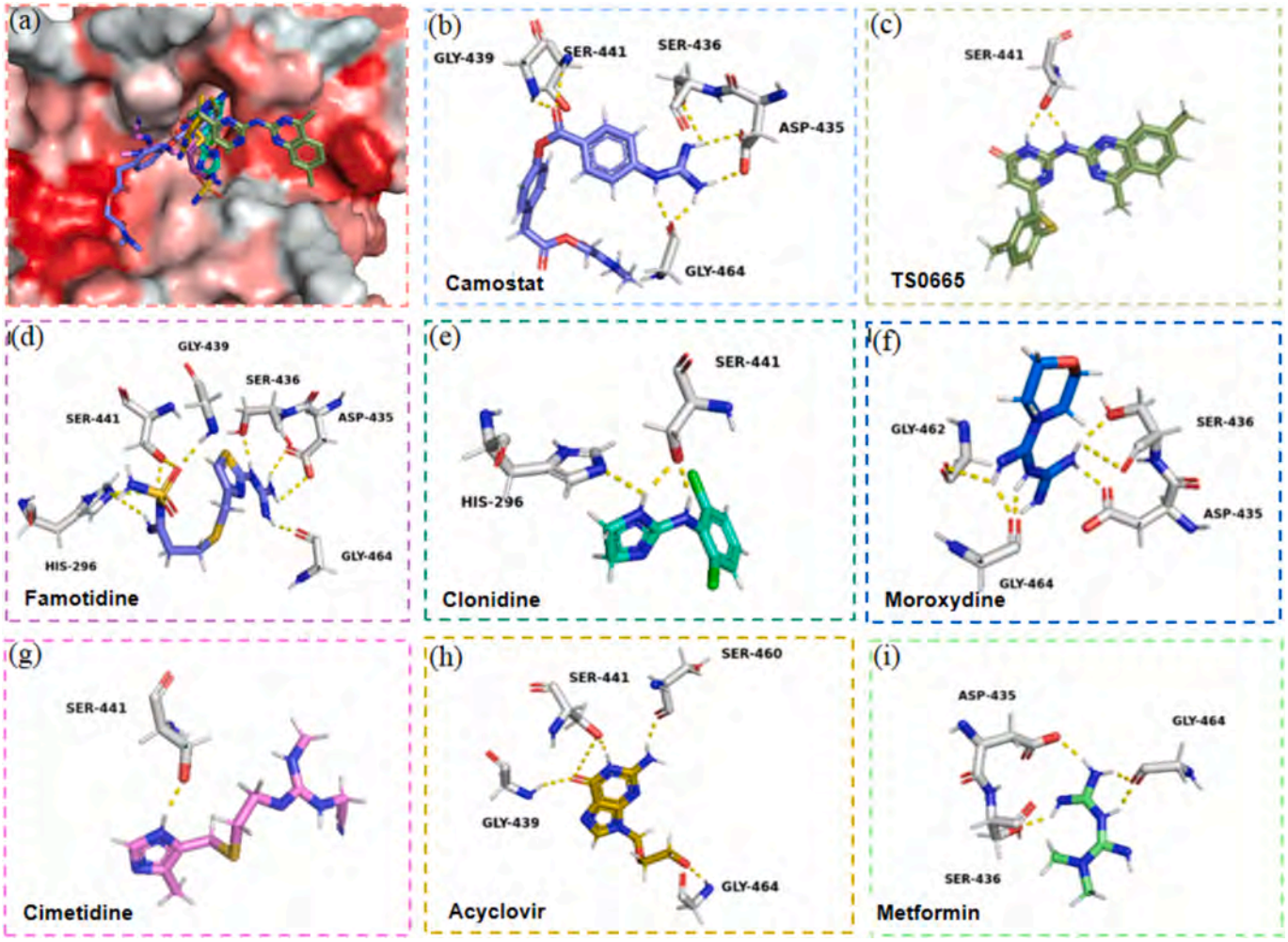


**Fig. 7.** Docking of compounds with TMPRSS2 virtual molecules. (a): TMPRSS2 active pocket and binding site with small molecules. (b): Camostat. (c): TS0665. (d): Famotidine. (e): Cimetidine. (f): Clonidine. (g): Moroxydine. (h): Acyclovir. (i): Metformin. The gray rod represents amino acid residues that interact with TMPRSS2 through hydrogen bonding, with numbers indicating amino acid residues and yellow dashed lines representing hydrogen bonds. (For interpretation of the references to colour in this figure legend, the reader is referred to the web version of this article.)

packing. The system suitability of the model was evaluated, and the results demonstrated favorable specificity and selectivity (Fig. 4a, b). Furthermore, compared to conventional physical adsorption columns, the prepared column exhibited an extended service life (Fig. 4c) and enhanced reproducibility (Table 2). In conclusion, the TMPRSS2-His-tag/CMC model proves to be effective and suitable for compound screening applications.

The model was employed to screen a library of 3010 small molecule compounds. To enhance screening efficiency, compounds were pooled into groups of ten and co-injected as mixed samples. The retention times of these pooled samples are presented in Fig. 5a. Based on a threshold of half the retention time of the positive control, pools exhibiting strong retention were selected for further individual analysis. The retention profiles from these single-compound screenings are shown in Fig. 5b.

Ultimately, 50 small molecule compounds (1.7 % of the total library) demonstrated stronger retention, including TS0665, TS1685, TS0422, and TS28310, among others. Representative chromatographic and chemical structures of selected compounds bound to the TMPRSS2-His-tag-CMC model are illustrated in Fig. 5c. These findings suggest that the identified compounds are potential TMPRSS2 ligands; however, further pharmacological studies are necessary to confirm their inhibitory activity against TMPRSS2.

### 3.3. Activity verification of potential active compounds

The inhibitory activity of the screened ligands against TMPRSS2 was evaluated using an intracellular enzyme activity assay. Compared with the control group, seventeen treatment groups exhibited varying degrees of inhibition on TMPRSS2 intracellular enzyme activity. Among these, compound TS0665 demonstrated significant inhibitory effects, achieving approximately 25 % inhibition at a concentration of 25 μmol/L (Fig. 6a).

Structural comparison between TS0665 and the known TMPRSS2 inhibitors camostat and nafamostat revealed that all three compounds show a similar guanidine moiety (Fig. 6b). This observation led to the hypothesis that the guanidine group may serve as a key pharmacophore responsible for the inhibitory activity against TMPRSS2.

To test this hypothesis, molecular docking was performed using six guanidine-containing drugs: famotidine, clonidine, mercaptopurine, cimetidine, acyclovir, and metformin (Fig. 7). The docking results indicated that the guanidine groups of TS0665, clonidine, cimetidine, and acyclovir form hydrogen bonds with SER441, while famotidine, mercaptopurine, and metformin interact via hydrogen bonding with ASP435, This finding aligns with the previously reported binding site of the drug on the TMPRSS2 receptor [31].

These findings suggest that the guanidine structure plays a crucial role in binding to key residues of TMPRSS2. To further validate this, the

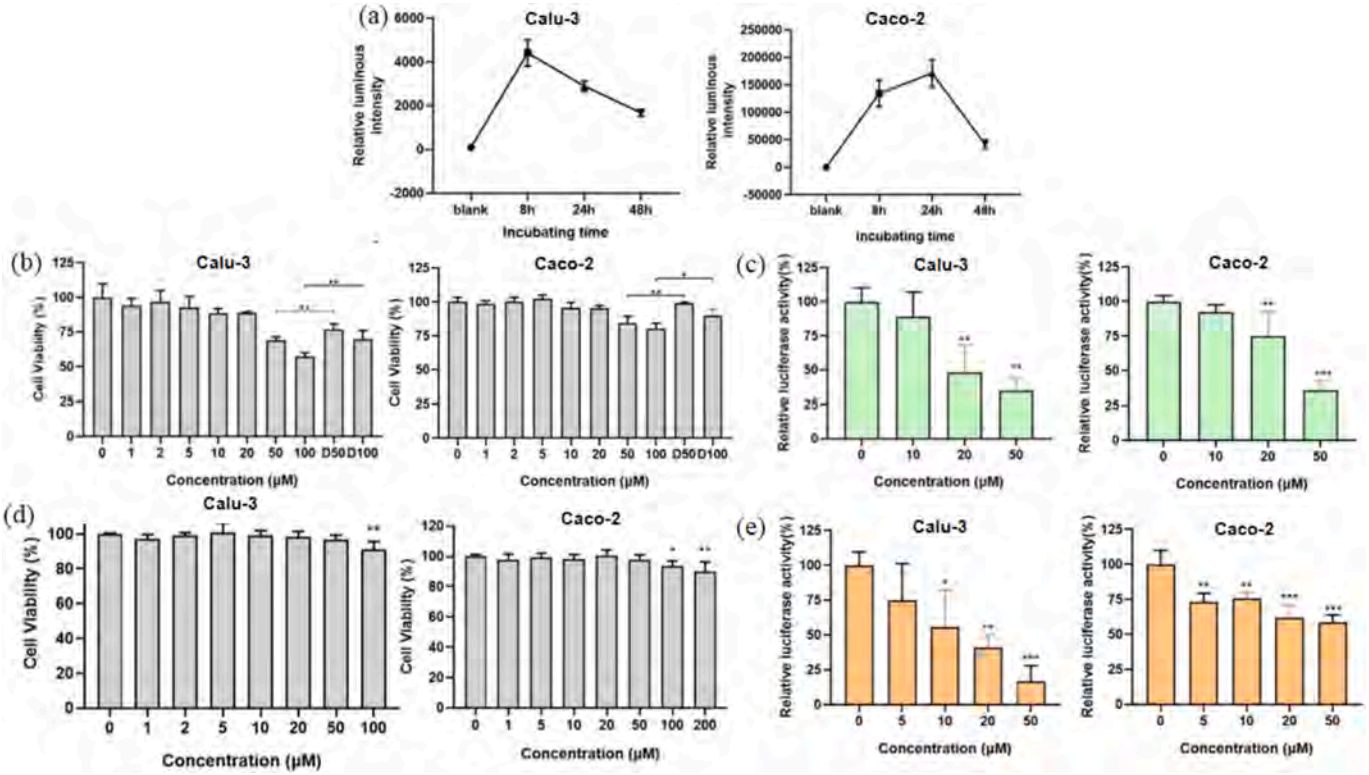


**Fig. 8.** Experimental results of pseudovirus infection of TS0665 and famotidine. (a): Experiment on the investigation of pseudovirus infection time, $n = 3$. (b): Cytotoxicity investigation experiment of TS0665, n = 3. D50 and D100 are DMSO treatment groups without compounds, and 0 is the control group. (c): The pseudovirus infection experiment of TS0665, $n = 5$. (d): Cytotoxicity investigation experiment of famotidine, n = 3. (e): The pseudovirus infection experiment of famotidine, n = 5; Compared with the control group* $P < 0.05$ , ** $P < 0.01$ , *** $P < 0.001$.

six guanidine-containing drugs were subjected to the TMPRSS2 intracellular enzyme activity assay. Compared to the control group, famotidine, mercaptopurine, cimetidine, acyclovir, and metformin showed significant inhibitory effects on TMPRSS2 enzymatic activity (Fig. 6a). Among these, famotidine demonstrated significant inhibitory effects, achieving approximately 30 % inhibition at concentration of 25 μmol/L. These results support the conclusion that guanidine-based compounds are promising candidates for inhibiting TMPRSS2 intracellular enzyme activity.

TS0665 and famotidine, which exhibited superior inhibitory effects in prior assays, were selected for further investigation using a pseudovirus infection model. First, the infection kinetics of the SARS-CoV-2 pseudovirus in Calu-3 and Caco2 cells were characterized. As shown in Fig. 8a, the peak fluorescence intensity in Calu-3 cells occurred at 8 h post-infection and gradually decreased thereafter, whereas in Caco2 cells, the highest relative luminescence was observed at 24 h. Consequently, 8 h and 24 h were selected as the respective infection endpoints for Calu-3 and Caco2 cells in subsequent pseudovirus experiments.

To evaluate the inhibitory effect of TS0665 on SARS-CoV-2 pseudovirus infection, its cytotoxicity was first assessed in two cell lines (Fig. 8b). TS0665 exhibited toxicity at a concentration of 50 μmol/L. Subsequent pseudovirus infection assays (Fig. 8c) revealed no inhibition at 10 μmol/L. However, at 20 μmol/L, the infection rates in Calu-3 and Caco2 cells were reduced to 55 ± 14 % and 67 ± 9 %, respectively. A further reduction to 35 ± 9 % and 35 ± 6 % was observed at 50 μmol/L.

Similarly, the cytotoxicity of famotidine was evaluated (Fig. 8d), which showed no significant toxicity in either cell line within the concentration range of 0–50 μmol/L. Pseudovirus infection experiments (Fig. 8e) demonstrated that famotidine reduced infection in Caco2 cells to between 59 % and 73 % across the same concentration range, though without clear concentration dependence. In contrast, a marked concentration-dependent inhibition was observed in Calu-3 cells: no significant effect was detected at 5 μmol/L, while infection rates decreased to 48 ± 13 %, 41 ± 9 %, and 17 ± 11 % at concentrations of 10, 20, and 50 μmol/L.

The results above demonstrate that both TS0665 and famotidine are capable of inhibiting SARS-CoV-2 pseudovirus infection in Calu-3 and Caco2 cells. Notably, famotidine exhibited superior inhibitory activity compared to TS0665. Furthermore, the antiviral effect of famotidine in Calu-3 cells was observed to be concentration-dependent.

## 4. Summary

This study successfully established a TMPRSS2 cell membrane chromatography screening model and applied it to screen a library of 3010 compounds. Two compounds, TS0665 and famotidine, were identified as potential inhibitors, which demonstrated significant anti-pseudovirus activity in pseudo virus infection assays. This model exhibits high throughput, strong selectivity, and good specificity, providing an effective platform for large-scale screening of TMPRSS2 small-molecule inhibitors. However, challenges such as limited column lifespan remain to be addressed. Furthermore, molecular docking simulations suggested that the guanidino group may play a critical role in TMPRSS2 inhibition. Future work can expand the evaluation of TMPRSS2 inhibitory activity for compounds containing this functional group, thereby facilitating the exploration of potential structure-activity relationships.

## CRediT authorship contribution statement

**Siqi Wang:** Writing – original draft, Formal analysis. **Min Si:** Investigation, Formal analysis, Data curation. **Qihuan Liao:** Methodology, Conceptualization. **Yifei Li:** Visualization, Software, Methodology. **Wenyu Yang:** Visualization, Validation, Software. **Huaizhen He:**

Resources, Project administration, Funding acquisition. **Cheng Wang:** Writing – review & editing, Supervision, Project administration.

## Declaration of competing interest

The authors declare that they have no known competing financial interests or personal relationships that could have appeared to influence the work reported in this paper.

## Acknowledgements

This research was funded by the National Natural Science Foundation of China (Grant No.82574376; 82150201) and the Special Practical Teaching Project of Xi'an Jiaotong University for Medical Undergraduates 2023 (No. 23SJZX-B12). Technical support in material characterization from the Instrumental Analysis Center (IAC) at Xi'an Jiaotong University gratefully acknowledged.

## Data availability

Data will be made available on request.

## References

[1] V. Mollica, A. Rizzo, F. Massari, The pivotal role of tmprss2 in coronavirus disease 2019 and prostate cancer, Future Oncol. 16 (27) (2020) 2029–2033, https://doi.org/10.2217/fon-2020-0571.
[2] J.M. Lucas, L. True, S. Hawley, M. Matsumura, C. Morrissey, R. Vessella, P. S. Nelson, The androgen-regulated type ii serine protease tmprss2 is differentially expressed and mislocalized in prostate adenocarcinoma, J. Pathol. 215 (2) (2008) 118–125, https://doi.org/10.1002/path.2330.
[3] C. Lim, T.V. Komarasamy, N. Adnan, A.K. Radhakrishnan, V. Balasubramaniam, Recent advances, approaches and challenges in the development of universal influenza vaccines, Influenza Other Respir. Viruses 18 (3) (2024) e13276, https://doi.org/10.1111/irv.13276.
[4] L. Yin, P. Rao, P. Elson, J. Wang, M. Ittmann, W.D. Heston, Role of tmprss2-erg gene fusion in negative regulation of psma expression, PLoS One 6 (6) (2011) e21319, https://doi.org/10.1371/journal.pone.0021319.
[5] K. Sakai, Y. Ami, M. Tahara, T. Kubota, M. Anraku, M. Abe, N. Nakajima, T. Sekizuka, K. Shirato, Y. Suzaki, A. Ainai, Y. Nakatsu, K. Kanou, K. Nakamura, T. Suzuki, K. Komase, E. Nobusawa, K. Maenaka, M. Kuroda, H. Hasegawa, Y. Kawaoka, M. Tashiro, M. Takeda, The host protease tmprss2 plays a major role in in vivo replication of emerging h7n9 and seasonal influenza viruses, J. Virol. 88 (10) (2014) 5608–5616, https://doi.org/10.1128/JVI.03677-13.
[6] G. Ragia, V.G. Manolopoulos, Inhibition of SARS-cov-2 entry through the ace2/tmprss2 pathway: a promising approach for uncovering early covid-19 drug therapies, Eur. J. Clin. Pharmacol. 76 (12) (2020) 1623–1630, https://doi.org/10.1007/s00228-020-02963-4.
[7] A. Heurich, H. Hofmann-Winkler, S. Gierer, T. Liepold, O. Jahn, S. Pohlmann, Tmprss2 and adam17 cleave ace2 differentially and only proteolysis by tmprss2 augments entry driven by the severe acute respiratory syndrome coronavirus spike protein, J. Virol. 88 (2) (2014) 1293–1307, https://doi.org/10.1128/JVI.02202-13.
[8] K. Shirato, M. Kawase, S. Matsuyama, Middle east respiratory syndrome coronavirus infection mediated by the transmembrane serine protease tmprss2, J. Virol. 87 (23) (2013) 12552–12561, https://doi.org/10.1128/JVI.01890-13.
[9] N. Kuhn, S. Bergmann, N. Kosterke, R. Lambertz, A. Keppner, J. van den Brand, S. Pohlmann, S. Weiss, E. Hummler, B. Hatesuer, K. Schughart, The proteolytic activation of (h3n2) influenza a virus hemagglutinin is facilitated by different type ii transmembrane serine proteases, J. Virol. 90 (9) (2016) 4298–4307, https://doi.org/10.1128/JVI.02693-15.
[10] Y.X. Lu, H.Q. Ju, F. Wang, L.Z. Chen, Q.N. Wu, H. Sheng, H.Y. Mo, Z.Z. Pan, D. Xie, T.B. Kang, G. Chen, J.P. Yun, Z.L. Zeng, R.H. Xu, Inhibition of the nf-kappab pathway by nafamostat mesilate suppresses colorectal cancer growth and metastasis, Cancer Lett. 380 (1) (2016) 87–97, https://doi.org/10.1016/j.canlet.2016.06.014.
[11] C. Zhiliang, Application of zebrafish in medcine screening, Chinese, J. Tradit. Chin. Med. 07 (40) (2015) 1235–1239.
[12] C.K. Maurer, M. Fruth, M. Empting, O. Avrutina, J. Hossmann, S. Nadmid, J. Gorges, J. Herrmann, U. Kazmaier, P. Dersch, R. Muller, R.W. Hartmann, Discovery of the first small-molecule csra-rna interaction inhibitors using biophysical screening technologies, Future Med. Chem. 8 (9) (2016) 931–947, https://doi.org/10.4155/fmc-2016-0033.
[13] X. Hou, S. Wang, T. Zhang, J. Ma, J. Zhang, Y. Zhang, W. Lu, H. He, L. He, Recent advances in cell membrane chromatography for traditional chinese medicines analysis, J. Pharm. Biomed. Anal. 101 (2014) 141–150, https://doi.org/10.1016/j.jpba.2014.05.021.
[14] S. Han, Y. Lv, L. Kong, Y. Sun, J. Fu, L. Li, L. He, Simultaneous identification of the anaphylactoid components from traditional chinese medicine injections using rat basophilic leukemia 2h3 and laboratory of allergic disease 2 dual-mixed/cell membrane chromatography model, Electrophoresis 39 (9–10) (2018) 1181–1189, https://doi.org/10.1002/elps.201700457.
[15] Y. Liu, X. Wang, Y. Gu, M. Zhang, Y. Cao, Z. Zhu, S. Lu, Y. Chai, X. Chen, Z. Hong, Covalent design of cell membrane stationary phase with enhanced stability for fast screening p-glycoprotein inhibitors, ACS Appl. Bio Mater. 3 (8) (2020) 5000–5006, https://doi.org/10.1021/acsabm.0c00514.
[16] F. Tsopelas, C. Stergiopoulos, P. Danias, A. Tsantili-Kakoulidou, Biomimetic separations in chemistry and life sciences, Mikrochim. Acta 192 (3) (2025) 133, https://doi.org/10.1007/s00604-025-06980-x.
[17] J. Drews, Drug discovery: a historical perspective, Science 287 (5460) (2000) 1960–1964, https://doi.org/10.1126/science.287.5460.1960.
[18] Y. Shan, J. Lu, H. Qian, Z. Xia, X. Mo, M. An, W. Yang, S. Wang, D. Che, C. Wang, H. He, Immobilized protein strategies based on cell membrane chromatography and its application in discovering active and toxic substances in traditional chinese medicine, Pharmacol. Res. 210 (2024) 107492, https://doi.org/10.1016/j.phrs.2024.107492.
[19] W. Ma, C. Wang, R. Liu, N. Wang, Y. Lv, B. Dai, L. He, Advances in cell membrane chromatography, J. Chromatogr. A 1639 (2021) 461916, https://doi.org/10.1016/j.chroma.2021.461916.
[20] X. Mo, C. Wang, Y. Shan, S. Wang, W. Yang, Z. Xia, Z. Qiao, T. Zhang, Y. Ding, R. Liu, H. He, L. He, Screening and discovery of volatile allergenic components from artemisia ordosica in Yulin region of northern China, J. Hazard. Mater. 494 (2025) 138759, https://doi.org/10.1016/j.jhazmat.2025.138759.
[21] J. Lu, Z. Xia, Y. Zhang, H. Wang, W. Yang, S. Wang, N. Wang, Y. Liu, H. He, C. Wang, L. He, "relative symmetry with electronegativity of different key-groups" strategy for mrgprx2 antagonist design and its effect on antigen-induced pulmonary inflammation, Acta Pharm. Sin. B 15 (1) (2025) 494–507, https://doi.org/10.1016/j.apsb.2024.11.023.
[22] J. Fu, Q. Jia, P. Liang, S. Wang, H. Zhou, L. Zhang, C. Gao, H. Wang, Y. Lv, S. Han, Targeting and covalently immobilizing the egfr through snap-tag technology for screening drug leads, Anal. Chem. 93 (34) (2021) 11719–11728, https://doi.org/10.1021/acs.analchem.1c01664.
[23] R.M. Garavito, S. Ferguson-Miller, Detergents as tools in membrane biochemistry, J. Biol. Chem. 276 (35) (2001) 32403–32406, https://doi.org/10.1074/jbc.R100031200.
[24] N. Bordag, S. Keller, Alpha-helical transmembrane peptides: a "divide and conquer" approach to membrane proteins, Chem. Phys. Lipids 163 (1) (2010) 1–26, https://doi.org/10.1016/j.chemphyslip.2009.07.009.
[25] Y.V. Grinkova, I.G. Denisov, S.G. Sligar, Engineering extended membrane scaffold proteins for self-assembly of soluble nanoscale lipid bilayers, Protein Eng. Des. Sel. 23 (11) (2010) 843–848, https://doi.org/10.1093/protein/gzq060.
[26] J.M. Dorr, S. Scheidelaar, M.C. Koorengevel, J.J. Dominguez, M. Schafer, C.A. van Walree, J.A. Killian, The styrene-maleic acid copolymer: a versatile tool in membrane research, Eur. Biophys. J. 45 (1) (2016) 3–21, https://doi.org/10.1007/s00249-015-1093-y.
[27] T.H. Bayburt, S.G. Sligar, Membrane protein assembly into nanodiscs, FEBS Lett. 584 (9) (2010) 1721–1727, https://doi.org/10.1016/j.febslet.2009.10.024.
[28] W. Kaplan, P. Husler, H. Klump, J. Erhardt, N. Sluis-Cremer, H. Dirr, Conformational stability of pgex-expressed schistosoma japonicum glutathione-transferase: a detoxification enzyme and fusion-protein affinity tag, Protein Sci. 6 (2) (1997) 399–406, https://doi.org/10.1002/pro.5560060216.
[29] H. Nikaido, Maltose transport system of escherichia coli: an abc-type transporter, FEBS Lett. 346 (1) (1994) 55–58, https://doi.org/10.1016/0014-5793(94)00315-7.
[30] A. Spriestersbach, J. Kubicek, F. Schafer, H. Block, B. Maertens, Purification of his-tagged proteins, Methods Enzymol. 559 (2015) 1–15, https://doi.org/10.1016/bs.mie.2014.11.003.
[31] X. Hu, J.H. Shrimp, H. Guo, M. Xu, C.Z. Chen, W. Zhu, A.V. Zakharov, S. Jain, P. Shinn, A. Simeonov, M.D. Hall, M. Shen, Discovery of tmprss2 inhibitors from virtual screening as a potential treatment of covid-19, Acs Pharmacol. Transl. Sci. 4 (3) (2021) 1124–1135, https://doi.org/10.1021/acsptsci.0c00221.